CANCER

YAP1 is a potent driver of the onset and progression of oral squamous cell carcinoma

Hirofumi Omori[1,2], Miki Nishio[1]*, Muneyuki Masuda[3]*, Yosuke Miyachi[1], Fumihito Ueda[1], Takafumi Nakano[3], Kuniaki Sato[2,4], Koshi Mimori[4], Kenichi Taguchi[5], Hiroki Hikasa[6], Hiroshi Nishina[7], Hironori Tashiro[8], Tohru Kiyono[9], Tak Wah Mak[10], Kazuwa Nakao[11], Takashi Nakagawa[2], Tomohiko Maehama[1†], Akira Suzuki[1,12†]

Head-and-neck squamous cell carcinoma (HNSCC) is the sixth most common group of cancers in the world, and patients have a poor prognosis. Here, we present data indicating that YAP1 may be a strong driver of the onset and progression of oral SCC (OSCC), a major subtype of HNSCC. Mice with tongue-specific deletion of *Mob1a/b* and thus endogenous YAP1 hyperactivation underwent surprisingly rapid and highly reproducible tumorigenesis, developing tongue carcinoma in situ within 2 weeks and invasive SCC within 4 weeks. In humans, precancerous tongue dysplasia displays YAP1 activation correlating with reduced patient survival. Combinations of molecules mutated in OSCC may increase and sustain YAP1 activation to the point of oncogenicity. Strikingly, siRNA or pharmacological inhibition of YAP1 blocks murine OSCC onset in vitro and in vivo. Our work justifies targeting YAP1 as therapy for OSCC and perhaps HNSCC, and our mouse model represents a powerful tool for evaluating these agents.

INTRODUCTION

Head-and-neck squamous cell carcinoma (HNSCC) is the sixth most common group of cancers in the world, affecting 600,000 people annually. About half of HNSCC patients die from their disease (*1*). The head and neck region of the body includes the oral cavity, larynx, and pharynx, all structures that are covered with squamous epithelium. Among HNSCC subtypes, oral SCC (OSCC) is the most frequent, and tongue cancers comprise a large proportion of OSCCs (*2*). Because 15% of HNSCC patients carry the human papillomavirus (HPV), HPV is considered to be one of the major causes of HNSCC. HPV (+) HNSCC usually occurs in the oropharynx, and patients with this malignancy have better prognoses or may even be cured (*1*). In contrast, the 85% of HNSCC that are HPV (−) are highly resistant to even intensified chemo/radiotherapy (*3*) as well as to currently available molecular targeting drugs (*4*). The fundamental molecular mechanisms underlying the onset and development of HPV (−) HNSCC have yet to be identified, hampering the generation of new therapeutic strategies.

The Cancer Genome Atlas (TCGA) project has revealed the presence of many altered gene exons in HNSCC (*2*). In HPV (−) HNSCC, *TP53* was highly mutated in 84% of cases. In addition, mutation of *FAT atypical cadherin1* (*FAT1*) was observed in 32%, *epidermal growth factor receptor* (*EGFR*) in 15%, and *Ajuba LIM protein* (*AJUBA*) in 7% of all HPV (−) HNSCC. Strikingly, these mutations were rare in HPV (+) HNSCC, with even *TP53* mutation at only 3%. Notably, mutations of *phosphoinositide 3 kinase, catalytic subunit alpha* (*PIK3CA*)/*phosphatase and tensin homolog* (*PTEN*; 50 to 60%) and *TP63* (20 to 30%) were commonly observed in both HPV (+) and HPV (−) HNSCC. Considering that HPV E6 strongly inactivates TP53 (*5*), TP53 inactivation must be a crucial and common oncogenic event in HNSCC. However, loss of *TP53* alone in mice never induces spontaneous HNSCC in vivo (*6*), meaning that other genetic and/or epigenetic alterations are also essential for HNSCC generation.

The core components of the Hippo pathway are the mammalian STE20–like (MST) kinases, large tumor suppressor homolog (LATS) kinases, nuclear Dbf2–related (NDR) kinase, and the adaptor proteins Salvador homolog 1 (SAV1) and Mps one binder kinase activator 1 (MOB1) (*7*). MOB1A/B are the adaptor proteins for both the LATS1/2 and NDR1/2 kinases, and by binding to LATS/NDR, MOB1A/B strongly increase the enzymatic activities of these kinases (*7*). Activated LATS/NDR kinases, in turn, phosphorylate Yes-associated protein 1 (YAP1) and transcriptional coactivator with PDZ-binding motif (TAZ; also known as WWTR1). YAP1/TAZ are key downstream transcriptional cofactors that act mainly on TEA domain transcription factors (TEADs) to regulate numerous target genes involved in cell growth and differentiation (*7*). After phosphorylation by LATS/NDR kinases, YAP1/TAZ are excluded from the nucleus and retained in the cytoplasm, where they are ubiquitylated by E3-ubiquitin ligase $SCF\beta^{TRCP}$ (also known as BTRC) and subjected to proteasome-mediated degradation (*7*). Thus, in most cell types, YAP1/TAZ are essentially positive regulators of cell proliferation that are negatively controlled by upstream Hippo core components. In vitro, YAP1/TAZ can be regulated by cell density, external mechanical forces, polarization, rigidity of the extracellular matrix, stress stimuli (*7*), or engagement of a G protein–coupled receptor (GPCR) by a soluble mediator (*7*). In vivo, YAP1 activation in mice results in organomegaly and tumor formation (*8*).

Several lines of evidence suggest a role for YAP1 in HNSCC. (i) Location 11q22 in the human *YAP1* locus is amplified in 8.6% of

[1]Division of Molecular and Cellular Biology, Kobe University Graduate School of Medicine, Hyogo, Japan. [2]Department of Otorhinolaryngology, Graduate School of Medical Sciences, Kyushu University, Fukuoka, Japan. [3]Department of Head and Neck Surgery, National Hospital Organization Kyushu Cancer Center, Fukuoka, Japan. [4]Department of Surgery, Kyushu University Beppu Hospital, Oita, Japan. [5]Department of Pathology, National Hospital Organization Kyushu Cancer Center, Fukuoka, Japan. [6]Department of Biochemistry, School of Medicine, University of Occupational and Environmental Health, Fukuoka, Japan. [7]Department of Developmental and Regenerative Biology, Medical Research Institute, Tokyo Medical and Dental University, Tokyo, Japan. [8]Department of Women's Health Sciences, Faculty of Life Sciences, Kumamoto University, Kumamoto, Japan. [9]Division of Carcinogenesis and Cancer Prevention, National Cancer Center Research Institute, Tokyo, Japan. [10]Princess Margaret Cancer Centre, University Health Network, Toronto, Ontario, Canada. [11]Medical Innovation Center, Graduate School of Medicine, Kyoto University, Kyoto, Japan. [12]Medical Institute of Bioregulation, Kyushu University, Fukuoka, Japan.
*These authors contributed equally to this work as second authors.
†Corresponding author. Email: tmaehama@med.kobe-u.ac.jp (T.M.); suzuki@med.kobe-u.ac.jp (A.S.)

HNSCC (*9*); (ii) YAP1 activity is associated with malignant phenotypes and poor prognosis both in vitro and in vivo (*9*, *10*); and (iii) mutations of *TP53*, *PIK3CA*/*PTEN*, *EGFR*, or *FAT1*, which are often observed in HNSCC, increase YAP1 activation in several cell types (*11*–*14*). HNSCC also frequently shows amplification of *TP63*, a master regulator of squamous cells, but the effect of this alteration on YAP1 activity is controversial (*15*, *16*).

We previously reported that *Mob1a/b* null mutant mice succumb to embryonic lethality at embryonic day 6.5 (*17*). We have also demonstrated that *Mob1a/b* loss induces extreme hyperactivation of endogenous YAP1/TAZ, resulting in the most severe phenotypes reported among mice mutated in Hippo core components in various tissues (*17*). Thus, MOB1A/B is a crucial hub in the Hippo signaling pathway. Because of the accumulating evidence in the literature on the importance of YAP1 in HNSCC progression, we generated tongue epithelium–specific *Mob1a/b* double knockout (tg*Mob1*DKO) mice and examined them to dissect the function of endogenous YAP1 in the onset and progression of the OSCC subtype of HNSCC. We demonstrate that hyperactivation of endogenous YAP1 induced by loss of *Mob1a/b* triggers surprisingly early onset and rapid progression of OSCC. Our data reveal that YAP1 is a powerful oncogenic driver of this malignancy.

RESULTS

Mob1a/b deletion in mouse tongue epithelium causes extremely rapid OSCC onset

To investigate the role of the Hippo-YAP1 pathway in mouse tongue epithelium in vivo, we used our previously generated strain of tamoxifen (TAM)–inducible *Mob1a/b*DKO mice [*Rosa26-CreERT*; $Mob1a^{flox/flox}$; $Mob1b^{-/-}$ (tg*Mob1*DKO) mice], which were created by mating *Rosa26-CreERT* transgenic (Tg) mice with $Mob1a^{flox/flox}$ and $Mob1b^{-/-}$ mice (*17*). Intraperitoneal injection of TAM into these animals causes early death at about 3 weeks due to widespread organ dysfunction, including hepatic failure (*17*). To extend mouse survival, we applied TAM directly and only to the tongue epithelium for 5 days starting on postnatal day 21 (P21; Fig. 1A and fig. S1A). *Cre*-mediated deletion of the floxed *Mob1a* gene was substantially

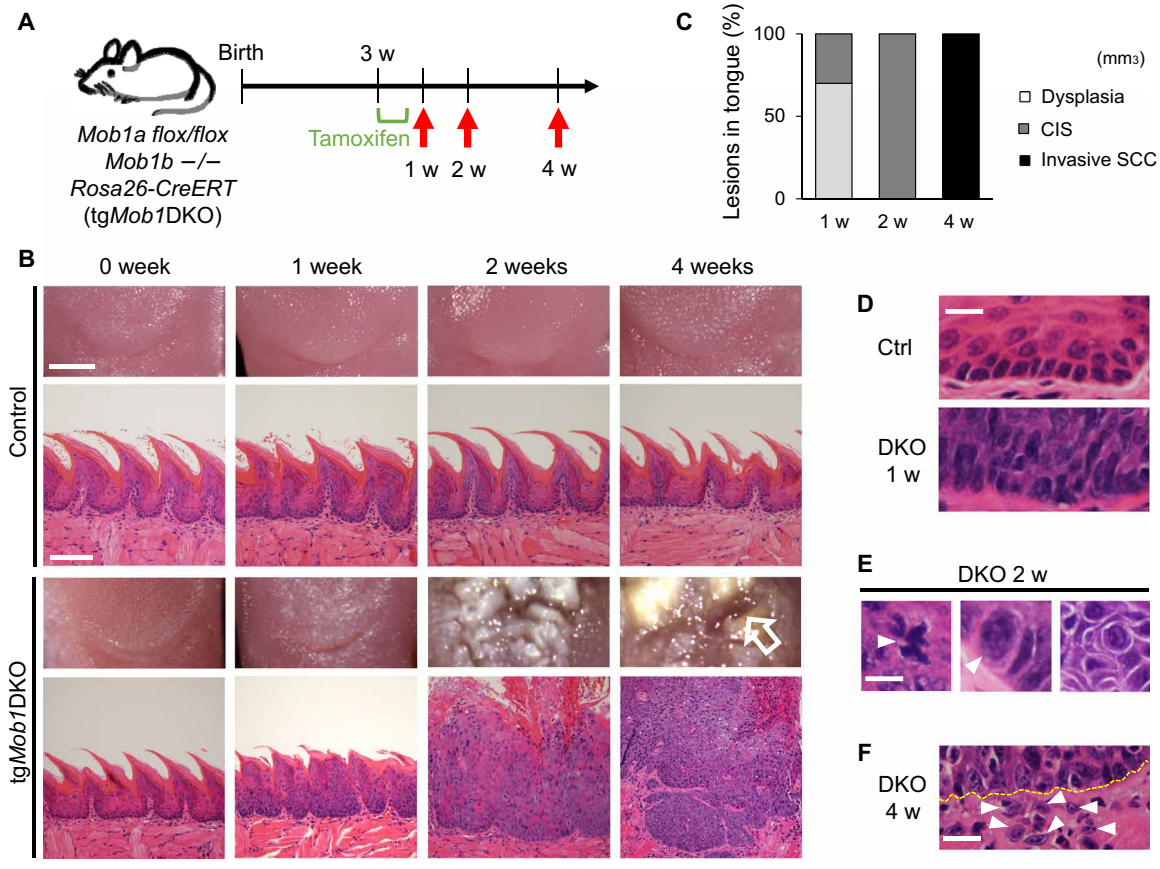

Fig. 1. Mob1a/b deletion in mouse tongue epithelium causes extremely rapid carcinogenesis. (**A**) Diagram of the protocol to generate tongue epithelial cell–specific *Mob1a/b* DKO mice (tg*Mob1*DKO). TAM was applied by a soft brush daily for 5 days to the tongues of 3-week-old $Mob1a^{flox/flox}$; $Mob1b^{-/-}$ (control) and *Rosa26-CreERT*; $Mob1a^{flox/flox}$; $Mob1b^{-/-}$ (mutant) mice. Mice were sacrificed at 1, 2, or 4 weeks (red arrows) after starting TAM application, and their tongue tissues were removed for histological analyses. (**B**) Representative macroscopic (small panels) and microscopic (large panels) views of H&E-stained sections of control (top) and tg*Mob1*DKO (bottom) tongue epithelial layers at the indicated weeks after starting TAM application. White arrow, deep ulcer formation. Scale bars, 1 mm (small panels) and 100 μm (large panels). Photo credit: Hirofumi Omori, Kobe University. (**C**) Percentages of the indicated lesion types present in the tongues of the mutant mice ($n = 10$ per group) in (B) at the indicated weeks after TAM. (**D**) H&E-stained sections of control and tg*Mob1*DKO tongue epithelium at 1 week after TAM. Moderate nuclear heterogeneity and loss of polarity are apparent in the mutants, indicating dysplasia. Scale bar, 5 μm. (**E**) H&E-stained sections of mutant tongue epithelium at 2 weeks after TAM showing atypical mitotic figures (left), nuclear enlargement (middle), and strongly heteromorphic cells (right), indicating CIS. Scale bar, 5 μm. (**F**) H&E-stained section of mutant tongue epithelium at 4 weeks after TAM revealing submucosal invasive SCC. White arrowheads, cancer cells penetrating beyond the basement membrane (yellow dashed line). Scale bar, 10 μm.

achieved by 3 days after the initiation of TAM application (fig. S1B), with the MOB1A and MOB1B proteins being essentially absent by day 7 after TAM (fig. S1C).

Macroscopically, the epithelial surface of tg*Mob1*DKO tongue showed mild roughness at 1 week after TAM, very rough mucosa accompanied by keratosis at 2 weeks after TAM, and deep ulceration at 4 weeks after TAM (Fig. 1B). To our surprise, by 1 week after TAM, histological examination revealed an increased number of polymorphic epithelial cells with hyperchromatic nuclei and loss of polarity, evidence of dysplasia (Fig. 1, C and D). Although Ki67 was expressed only in the basal cells of the tongue epithelium before TAM treatment, the percentage of Ki67-positive cells among polymorphic epithelial cells increased markedly by 1 week after TAM (fig. S1D), demonstrating the increased proliferative capacity of MOB1-deficient epithelial cells. Atypical mitotic figures (Fig. 1E, left), nuclear enlargement (Fig. 1E, middle), and strongly heteromorphic cells (Fig. 1E, right) indicative of carcinoma in situ (CIS) were observed in the tongue as early as 1 week after TAM (Fig. 1C and fig. S1E). All mice developed tongue CIS by 2 weeks after TAM (Fig. 1, B, C, and E), and all mice developed invasive SCC by 4 weeks after TAM (Fig. 1, B, C, and F). Almost all of these SCC-bearing mutants died by 8 weeks after TAM, most likely due to malnutrition caused by their dysphagia. Because there were no significant histological differences among *Mob1a*$^{+/+}$; *Mob1b*$^{+/+}$ mice treated with TAM, *Rosa26-CreERT*; *Mob1a*$^{+/+}$; *Mob1b*$^{+/+}$ mice with TAM, *Rosa26-CreERT*; *Mob1a*$^{flox/flox}$; *Mob1b*$^{-/-}$ mice without TAM, and *Mob1a*$^{flox/flox}$; *Mob1b*$^{-/-}$ mice with TAM (fig. S1F), we used *Mob1a*$^{flox/flox}$; *Mob1b*$^{-/-}$ mice with TAM as controls for subsequent experiments unless otherwise stated. These studies were designed to explore why altered Hippo signaling induced the extremely rapid onset of tongue cancers.

Tumorigenic properties of *Mob1a/b*-deficient tongue epithelial cells

We established a TAM-inducible *Mob1a/b*DKO tongue epithelial cell line (*iMob1*DKO cells) and treated them in vitro with (+) or without (−) TAM. Compared to control *iMob1*DKO−TAM cells, *iMob1*DKO+TAM cells showed increased cell proliferation and saturation density (Fig. 2A). When cultures of these overconfluent *iMob1*DKO+TAM cells were stained to detect the tight junction protein ZO-1, we found only weak staining of this protein in the tight junctions, indicating impaired cell polarity (fig. S2A). In contrast, cultures of *iMob1*DKO−TAM cells showed normal ZO-1 staining in the tight junctions. Because there was no difference in cell size between *iMob1*DKO+TAM and *iMob1*DKO−TAM cells (fig. S2B), we concluded that cell-cell contact inhibition was impaired in the absence of *Mob1a/b*. In addition, the number of apoptotic cells was decreased in the mutant culture compared to the control (Fig. 2B). Next, to determine how MOB1 inactivation affected the self-renewal of tongue epithelial stem cells, we quantified the capacity of control (−TAM) and mutant (+TAM) *iMob1*DKO cells to form colonies in culture. A lack of *Mob1a/b* induced a 2.2-fold increase in colony-forming efficiency (Fig. 2C, left panels). When these primary colonies were replated to test their ability to form secondary colonies, a 2.8-fold increase in secondary colony-forming efficiency was observed in the absence of *Mob1a/b* (Fig. 2C, right panels). A comparison of cell cycle and cell ploidy in *iMob1*DKO−TAM versus *iMob1*DKO+TAM cells revealed a decrease in G_0-G_1 phase cells and increases in S phase cells and aneuploid cells in the mutant culture (Fig. 2D). Indirect immunofluorescence (IF) analysis of control and mutant cells using anti–γ-tubulin and anti–α-tubulin antibodies uncovered increases in multipolar spindle formation (Fig. 2E) and micronuclei (Fig. 2F) in mutant cells, indicating chromosomal instability. Thus, the increases in cell proliferation and stem cell self-renewal observed in the absence of *Mob1a/b*, coupled with chromosomal instability, resistance to apoptosis, and inadequate cell contact inhibition, may underlie the rapid onset and development of tongue cancer in TAM-treated tg*Mob1*DKO mice.

Onset of OSCC depends on activation of YAP1 rather than TAZ

We next investigated the biochemical effects of *Mob1a/b* loss on Hippo components in *iMob1*DKO cells that were left untreated or treated with TAM for 7 days. As expected, *iMob1*DKO+TAM cells showed a reduction in LATS1 protein and an increase in the total protein levels of YAP1. Protein levels of several representative direct transcriptional targets of YAP1, including connective tissue growth factor (CTGF), baculoviral IAP repeat-containing protein 5 (BIRC5), and topoisomerase II-alpha (TOP2A), were also significantly elevated. However, there was no effect on total TAZ protein (Fig. 3A). Furthermore, YAP1 was predominantly localized in the nuclei of *iMob1*DKO+TAM cells even when cultured under high–cell density conditions (Fig. 3B). Thus, YAP1 hyperactivation is a prominent feature of mutant tongue epithelial cells prone to OSCC development.

To clarify the role of YAP1 in OSCC-related phenotypes, we generated strains of triple KO mice lacking MOB1A/B plus YAP1 (tg*Yap1*TKO), or lacking MOB1A/B plus TAZ (tg*Taz*TKO). Unlike tg*Mob1*DKO mice, which all develop invasive SCC at 4 weeks after TAM, MOB1A/B-deficient mice also lacking YAP1 showed only mild to moderate dysplasia in the tongue (Fig. 3C and fig.S2C). In contrast, MOB1A/B-deficient mice also lacking TAZ developed a highly aggressive form of invasive SCC, with some lesions penetrating from the tongue surface into the floor of mouth. The measured depth of invasion of malignant cells into the mouth floor was significantly increased in tg*Taz*TKO mice compared to tg*Mob1*DKO mice (Fig. 3D). In addition, immunohistochemical (IHC) staining to detect YAP1/TAZ revealed that tg*Mob1*DKO mice showed increased frequency of nuclear YAP1 localization compared to controls, but no alteration in the frequency of nuclear TAZ (fig. S2C). These results were further confirmed by IHC staining to visualize YAP1 or TAZ in the tongues of tg*Yap1*TKO and tg*Taz*TKO mice (fig. S2C). Thus, the MOB1A/B-deficient phenotype is largely dependent on YAP1 rather than on TAZ.

The SRC family inhibitor dasatinib prevents the onset of tg*Mob1*DKO-induced tongue cancer in mice

We speculated that inhibition of YAP1 hyperexpression might prevent the development of tongue cancer in our tg*Mob1*DKO mice. To choose a compound to exert YAP1 inhibition in vivo, we first tested the effects of the candidate compounds dasatinib, simvastatin, verteporfin, and the Rock inhibitor Y-27632 on YAP1 protein expression in the human OSCC cell line HSC4 (fig. S3A). We also evaluated the effects of these drugs on YAP1 activity in H1299-Luc cells in a reporter assay (fig. S3B). Dasatinib was the most effective YAP1 inhibitor in both of these assays, guiding us to choose dasatinib for our in vivo experiments. Biochemically, dasatinib is a multikinase inhibitor that efficiently blocks Src family kinases such as SRC, LCK, YES, and FYN (*18*). SRC directly and indirectly activates YAP1, and inhibition of SRC by dasatinib has been shown to efficiently suppress YAP1 activation (*19*).

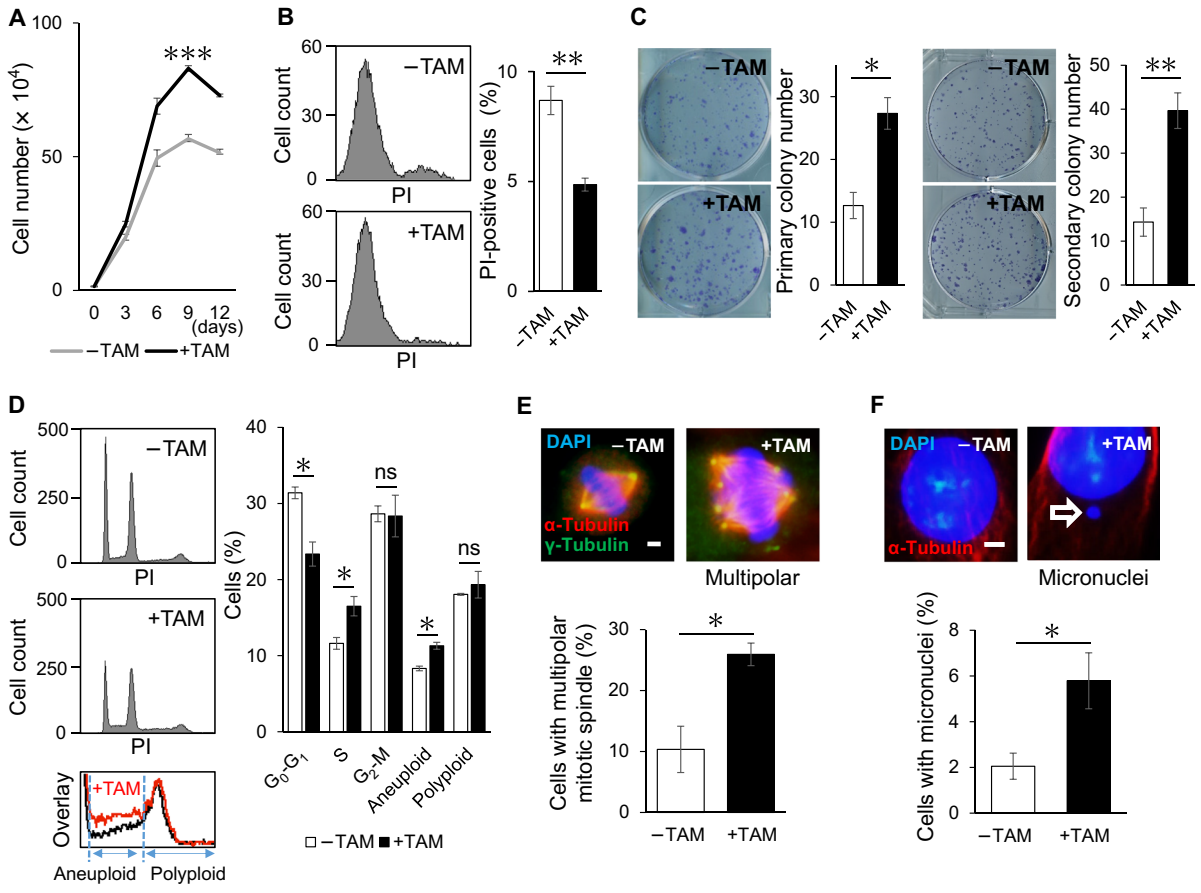

Fig. 2. Tumorigenic anomalies in Mob1a/b DKO tongue epithelial cells. (**A**) Absolute numbers of *iMob1*DKO tongue epithelial cells that were left untreated (control; *iMob1*DKO–TAM cells) or treated with 0.5 μM TAM for 3 days (*iMob1*DKO+TAM cells) and then grown for the indicated number of days in the absence of TAM. (**B**) Flow cytometry (left) and quantitation (right) of propidium iodide (PI)–positive dead cells in the cultures in (A). (**C**) *iMob1*DKO cells were treated in vitro with TAM (0.5 μM) for 3 days (+TAM) or left untreated (–TAM) and serially plated to generate first primary colonies and then secondary colonies. Crystal violet staining (left) and colony counts (right) of primary (left side) and secondary (right side) colonies were performed on day 7 after plating. Photo credit: Hirofumi Omori, Kobe University. (**D**) Top left: DNA content frequency histograms of control (*iMob1*DKO–TAM) and *Mob1a/b* mutant (*iMob1*DKO+TAM) tongue epithelial cells. Right: Percentage of cells from the top left panels in the G_0-G_1, S, and G_2-M phases of the cell cycle as determined by fractional DNA content. Bottom left: Overlay of aneuploid and polyploid cell numbers for the cells in the right panel. (**E** and **F**) Top: Immunostaining to detect γ-tubulin (green) and α-tubulin (red) in control (*iMob1*DKO–TAM) and mutant (*iMob1*DKO+TAM) tongue epithelial cells. DAPI (blue), nuclei. Scale bars, 1 μm. Multipolar spindles and micronuclei (white arrow) were detected in mutant cells. Bottom: Quantitation of the percentage of cells in the top panels showing multipolar spindles (E) and micronuclei (F). Data are shown as means ± SEM of triplicate samples. **P* < 0.05, ***P* < 0.01, and ****P* < 0.001, *t* test. ns, not significant; i.p., intraperitoneally.

To investigate the effect of pharmacological YAP1 inhibition on our TAM-inducible tg*Mob1*DKO mice, we treated these animals with dasatinib or dimethyl sulfoxide (DMSO; vehicle control) 3 days before applying TAM ointment to the tongue (Fig. 4A). The mice were then sacrificed at 2 weeks after TAM. We found that dasatinib treatment strongly blocked both YAP1 protein expression (Fig. 4B) and the excessive cell proliferation associated with YAP1 hyperactivation (Fig. 4C). Macroscopically, the mucosal irregularity accompanied by keratinization obvious in tg*Mob1*DKO+TAM mice had improved after dasatinib treatment (Fig. 4D). Histological examination of tongue epithelial cells revealed that, whereas DMSO-treated control mice all developed CIS at 2 weeks after TAM, the onset of CIS in dasatinib-treated mice was completely blocked, although a mild or moderate dysplasia was still present (Fig. 4D). Thus, dasatinib inhibits the onset of YAP1-induced tongue carcinomas. To confirm this effect of YAP1 inhibition in vivo, we treated tg*Mob1*DKO+TAM mice with simvastatin in the same fashion and observed results similar to those achieved with dasatinib (fig. S3C). These data suggest that drug-mediated inactivation of YAP1 could be of therapeutic benefit in OSCC.

Inhibition of YAP1 slows the progression of OSCC

Our findings that YAP1 activation causes very early OSCC onset, and that loss of YAP1 prevents the appearance of these tumors, prompted us to theorize that YAP1 must be a potent oncogenic initiator of OSCC. We next investigated whether YAP1 plays a crucial role in not only tumor initiation but also tumor progression. We engineered the human OSCC cell line SCC9, which features only low YAP1 expression (fig. S4, A and B), to overexpress YAP1 by transfecting it with a plasmid driving expression of the constitutively active YAP1-5SA mutant protein (fig. S4C). YAP1-overexpressing SCC9 cells showed greatly enhanced proliferation in vitro (Fig. 4E). We then transfected HSC4 cells, which naturally feature strong YAP1 expression (fig. S4, A and B), with *YAP1* small interfering RNA (siRNA; fig. S4D) or treated them with a YAP1 inhibitor such as

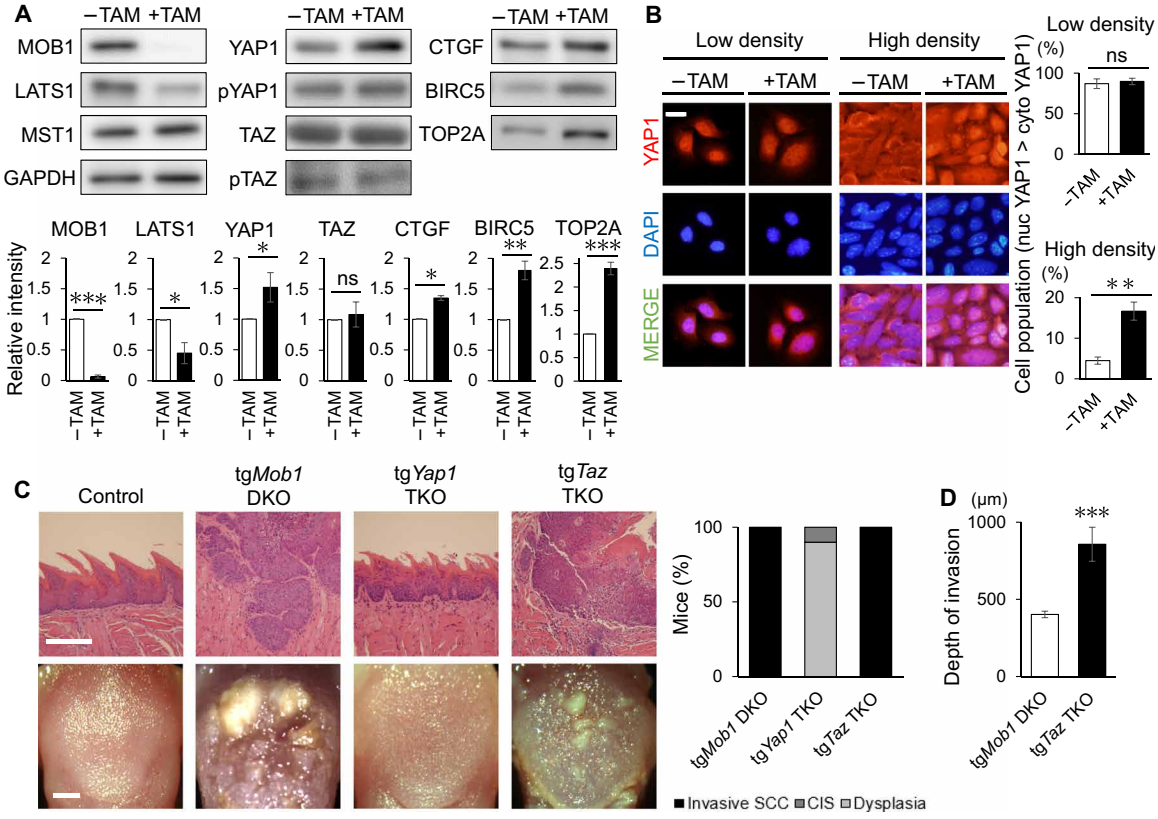

Fig. 3. Involvement of the *Mob1a/b-Lats-Yap1* pathway in OSCC. (**A**) Top: Immunoblots to detect the indicated proteins in total extracts of *iMob1*DKO tongue epithelial cells that were left untreated (–TAM; control) or treated with TAM (+TAM) for 7 days. GAPDH, loading control. Bottom: Densitometric relative quantitation of the indicated proteins in the blots in the top panels. (**B**) Left: Immunostaining to detect YAP1 in *iMob1*DKO–TAM and *iMob1*DKO+TAM tongue epithelial cells that were plated at low or high cell density. Scale bar, 10 μm. Right: Percentages of cells in the cultures in the left panels that showed higher YAP1 levels in the nucleus (nuc YAP1) than in the cytoplasm (cyto YAP1). (**C**) Left: Representative H&E-stained sections (top panels) and macroscopic views (bottom panels) of tongue epithelium from control, tg*Mob1*DKO, tg*Yap1*TKO (tg*Mob1*DKO plus *Yap1* KO), and tg*Taz*TKO (tg*Mob1*DKO plus *Taz* KO) mice at 4 weeks after TAM ($n = 10$ mice per group). Scale bars, 100 μm (top panels) and 1 mm (bottom panels). Right: Percentages of mice in the left panels displaying the indicated lesions. Photo credit: Hirofumi Omori, Kobe University. (**D**) Quantitation of SCC invasion depth in tongue epithelium of the mice in (C). The depth of invasion was measured from the level of the nearest adjacent normal mucosa to the extent of the deepest tumor invasion into the tongue musculature. Data are shown as means ± SEM of triplicate samples. *$P < 0.05$, **$P < 0.01$, and ***$P < 0.001$, *t* test.

dasatinib, simvastatin, or verteporfin. In all these cases, YAP1 inhibition significantly suppressed HSC4 cell proliferation in vitro (Fig. 4, F and G). Moreover, siRNA-mediated YAP1 knockdown enhanced the sensitivity of HSC4 cells to the chemotherapeutic cisplatin (fig. S4E), implying that combining a YAP1 inhibitor with cisplatin might be an attractive new approach for OSCC therapy.

To examine the effects of YAP1 inhibition in vivo, we first xenografted doxycycline (Dox)–inducible sh*YAP1*-transfected HSC4 cells (fig. S4F) into *nude* mice, which were then supplied with normal drinking water (control) or water containing Dox. We found that Dox-induced inhibition of YAP1 expression efficiently suppressed the ability of these modified HSC4 cells to grow into tumors in vivo (Fig. 4H). We then xenografted unmodified HSC4 cells into *nude* mice and treated these animals with DMSO or dasatinib. Again, blocking YAP1 activity decreased OSCC development in these mice (Fig. 4I).

Last, we applied these findings to our TAM-induced tg*Mob1*DKO mouse model of tongue cancer. We treated TAM-inducible tg*Mob1*DKO mice with dasatinib soon after CIS onset at 2 weeks after TAM (Fig. 4J). Tumor cell proliferation was inhibited compared to DMSO-treated controls (Fig. 4K), and the progression of these lesions into invasive tongue cancer had slowed significantly at 4 weeks after TAM (Fig. 4L). Histological analysis revealed that there was no significant increase in TUNEL$^+$ (terminal deoxynucleotidyl transferase–mediated deoxyuridine triphosphate nick end labeling–positive) cells in the tongues of dasatinib-treated tg*Mob1*DKO+TAM mice, indicating that dasatinib did not increase apoptosis but rather blocked cell proliferation (fig. S4G).

Together, these data indicate that endogenous YAP1 hyperactivation is involved in both OSCC onset and progression and is a driving force in tongue cancer in mice and humans. These results further strengthen our contention that YAP1 inhibitors may be promising novel agents for OSCC therapy.

Step-wise YAP1 activation in human tongue cancers

Previous reports had suggested that nuclear localization of YAP1 was frequently observed at the precancerous stage of human OSCC (*10*). We obtained samples of nontumorous tongue tissue (NT-control) and tongue dysplasia, CIS, or invasive SCC from 86 patients at the National Hospital Organization Kyushu Cancer Center. These samples were immunostained to detect YAP1, and YAP1 levels were quantified using a grade scale (see Fig. 5A and Materials and Methods). As

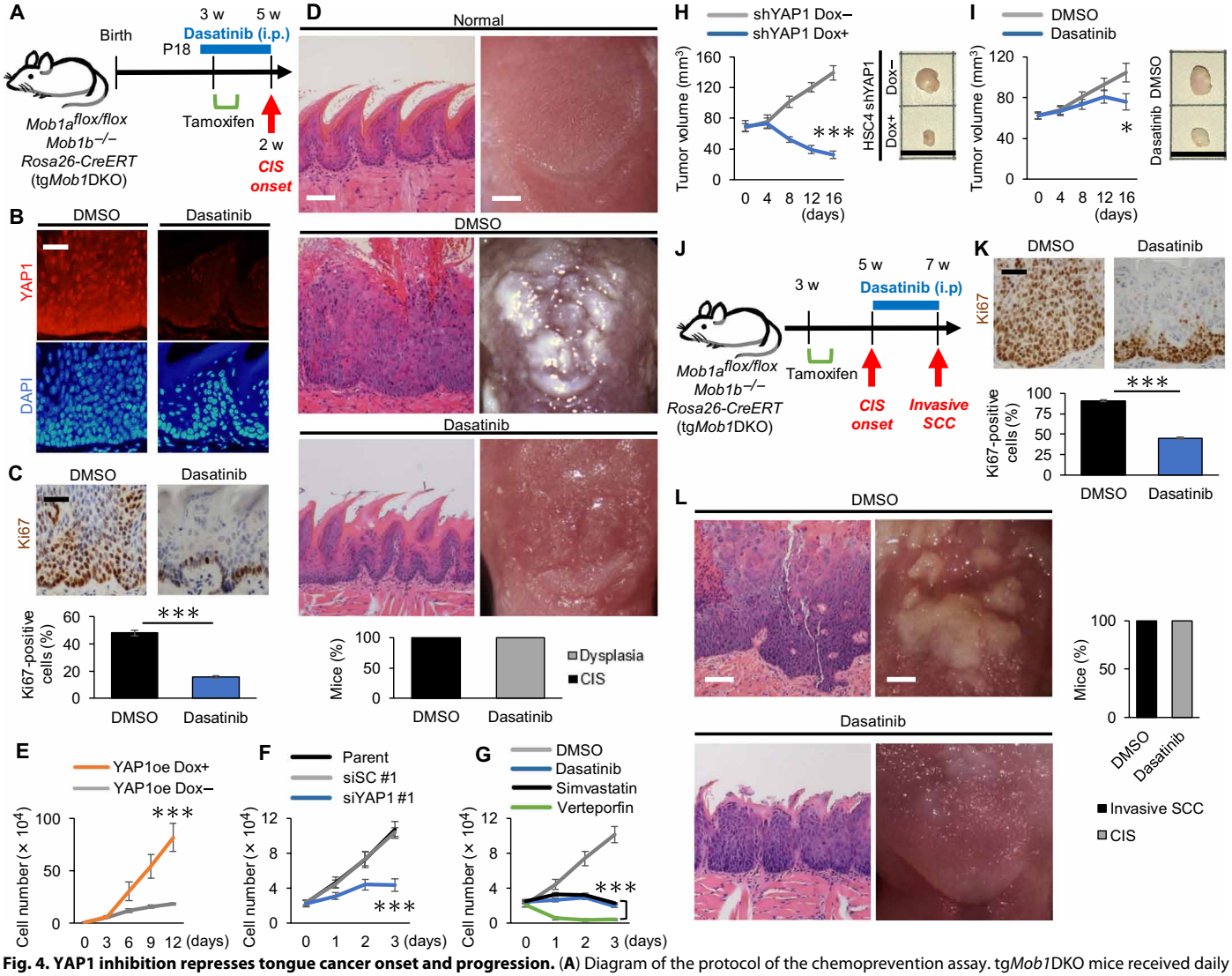

Fig. 4. YAP1 inhibition represses tongue cancer onset and progression. (**A**) Diagram of the protocol of the chemoprevention assay. tg*Mob1*DKO mice received daily intraperitoneal injection of dasatinib or DMSO (control; $n = 6$ per group) for a total of 17 days starting 3 days (P18) before TAM application on P21. Mice were sacrificed at 2 weeks after TAM. (**B**) Representative images of IF detection of YAP1 in tongue epithelium from the dasatinib- or DMSO-treated mice in (A). Scale bar, 50 μm. (**C**) Top: Representative Ki67 immunostaining of tongue epithelium from the mice in (A). Scale bar, 50 μm. Bottom: Percentages of Ki67-positive cells in the sections in the top panels. (**D**) Top: Representative H&E staining of sections (left panels) and macroscopic views (right panels) of tongues from DMSO-treated ($n = 6$) or dasatinib-treated ($n = 6$) tg*Mob1*DKO mice after 2 weeks of treatment. Scale bars, 100 μm (left panels) and 1 mm (right panels). Normal, H&E-stained section of a tongue from a tg*Mob1*DKO mouse treated with DMSO but not TAM (control). Bottom: Percentages of the DMSO- or dasatinib-treated mice in (A) showing the indicated lesions. Photo credit: Hirofumi Omori, Kobe University. (**E**) Growth in culture of SCC9 cells that Dox-inducibly overexpressed constitutively active YAP1 (YAP1-5SA) and were treated (+) or not (–) with Dox. (**F** and **G**) Growth in culture of HSC4 cells that were left untreated (parent) or treated with (F) si-scramble (siSC#1; control) or si*YAP1*#1 or (G) DMSO (control), dasatinib, verteporfin, or simvastatin. (**H** and **I**) Left: Volumes of tumors in *nude* mice ($n = 12$ per group) that were xenografted subcutaneously with (H) Dox-inducible sh*YAP1*-expressing HSC4 cells or (I) unmodified HSC4 cells. Mice were supplied with (H) normal drinking water or water containing Dox (2 mg/ml), or (I) DMSO or dasatinib that was administered intraperitoneally on day 10 when tumors became visible. Right: Representative macroscopic view of the tumors evaluated in the left panels of (H) and (I) at 16 days after treatment. Scale bars, 10 mm. (**J**) Diagram of the protocol of the chemotherapy assay. tg*Mob1*DKO mice received daily intraperitoneal injection of dasatinib or DMSO ($n = 6$ per group) for 2 weeks starting at 2 weeks after TAM. Mice were sacrificed at 7 weeks of age immediately at treatment end (right red arrow). (**K**) Top: Representative Ki67 immunostaining of tongue epithelium from the mice in (J) after 2-week treatment. Scale bar, 50 μm. Bottom: Percentage of Ki67-positive cells in the sections in the top panels. (**L**) Left: H&E-stained sections (left panels) and macroscopic views (right panels) of the tongues of the mice in (J) after 2-week treatment. Scale bars, 100 μm (left panels) and 1 mm (right panels). Right: Percentages of the mice in (J) whose tongues exhibited the indicated lesions after 2-week treatment. Photo credit: Hirofumi Omori, Kobe University. Data are shown as means ± SEM. *$P < 0.05$ and ***$P < 0.001$, *t* test.

expected, NT-control epithelium showed weak YAP1 expression (mean grade = 0.7) only in the basal layer, with negligible YAP1 expression above the basal layer (Fig. 5, A and B). Most patients with tongue dysplasia showed enhanced YAP1 expression (mean grade = 3.5) in the nonbasal upper layer, indicating that YAP1 expression is higher than in controls from the early precancerous stage. Patients with CIS in the tongue displayed stronger nuclear staining of YAP1 than dysplastic patients, and patients with invasive SCC exhibited much more intense YAP1 staining than either of these (Fig. 5, A and B). We next tested for YAP1 activation using IHC

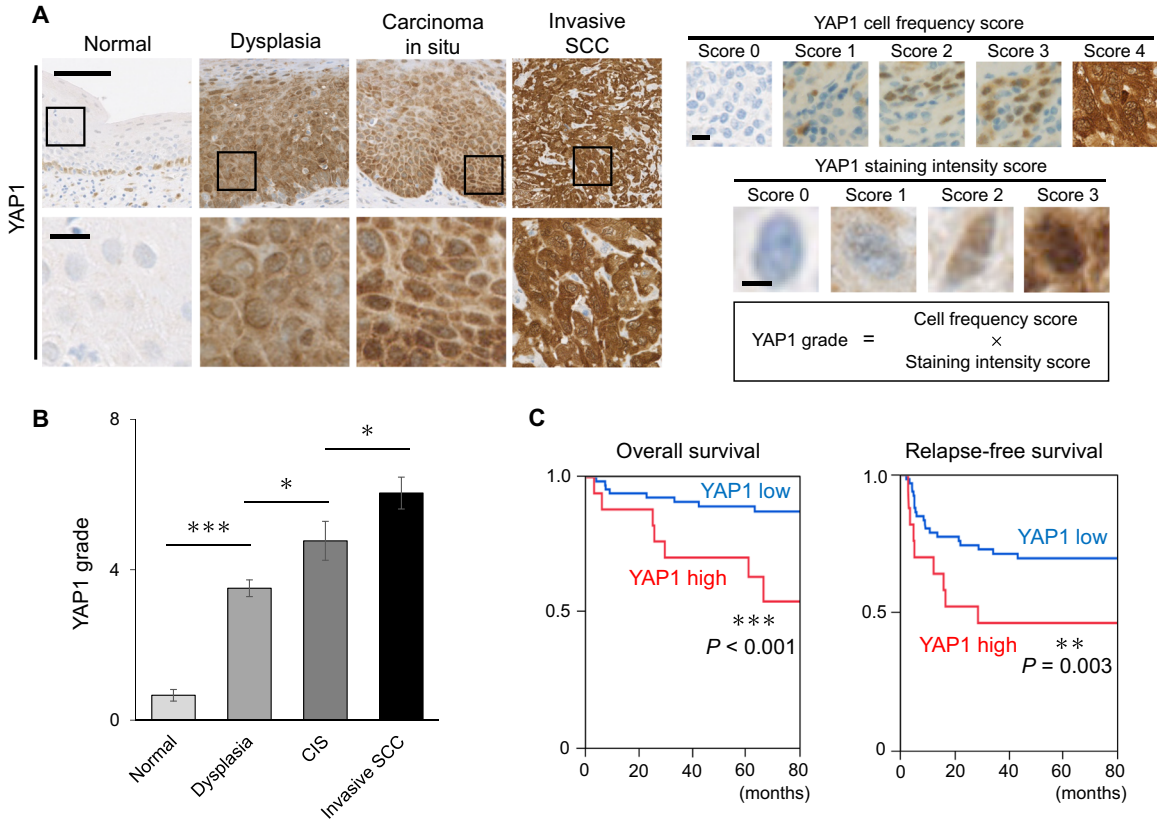

Fig. 5. Characterization of YAP1 activation in human OSCC specimens. (**A**) Left: Low-magnification (top panels; scale bar, 40 μm) and high-magnification (bottom panels; scale bar, 10 μm) views of representative YAP1-immunostained plus hematoxylin-counterstained sections of normal human tongue (mean YAP1 activity grade = 0.67; $n = 56$), dysplasia (mean grade = 3.5; $n = 63$), CIS (mean grade = 4.8, $n = 26$), and invasive SCC (mean grade = 6.4, $n = 86$). Right: Determination of YAP1 grade. Representative sections from the left panels were scored for YAP1 frequency and intensity as indicated. Scale bars, 10 μm (frequency) and 3 μm (intensity). The YAP1 grade was the product of these scores (see Materials and Methods). (**B**) Compilation of YAP1 grade scores in sections of human normal tongue, and tongues with dysplasia, CIS, or invasive SCC. Data are shown as means ± SEM. *$P < 0.05$ and ***$P < 0.001$, *t* test. (**C**) Kaplan-Meier curves showing overall survival (left) and relapse-free survival (right) of 86 tongue cancer patients who underwent surgical resection. The patients were divided into a high YAP1 expression group ($n = 14$) and a low YAP1 expression group ($n = 72$; see table S1). **$P < 0.01$ and ***$P < 0.001$, Wilcoxon test.

evaluation of the expression of the YAP1 target genes CTGF, BIRC5, and TOP2A. In examining 14 OSCC specimens with high YAP1 protein levels and 14 specimens with low YAP1 protein levels, we found that CTGF protein tended to rise in the YAP1-high group (fig. S5A), and that the BIRC5 (fig. S5B) and TOP2A (fig. S5C) proteins were increased significantly in these same specimens. Thus, YAP1 activation appears to have a very important function in the onset and progression of tongue cancer not only in mice but also in humans.

We then looked at the effect of high YAP1 expression on the overall survival and relapse-free survival of human tongue cancer cases. We examined the histories of our 86 selected tongue cancer patients, each of whom had undergone surgical resection at the National Hospital Organization Kyushu Cancer Center. We found that high YAP1 expression in human tongue cancer patients ($n = 14$) correlated with lymph node metastasis (table S1), decreased overall survival (Fig. 5C, left), and reduced relapse-free survival (Fig. 5C, right). Thus, elevated YAP1 activity in human tongue cancer is a negative prognostic indicator.

Molecules mutated in human HNSCC can activate YAP1

Human HNSCCs often bear mutations of *TP53*, elements of PI3K/PTEN signaling, *FAT1*, or elements of EGFR signaling (*2*). All of these entities have been previously reported to activate YAP1 in one or more cell types (*11*–*14*). Mutation of *TP63*, a master regulator of squamous cells, is also frequently observed in human HNSCC, but its effects on YAP1 remain under debate (*15*, *16*). We hypothesized that one or more of these mutations would activate YAP1 in transformed epithelial cells from an OSCC patient.

The WSU-HN30 human HNSCC cell line is HPV (−), low in EGFR, and wild type for *TP53*, *FAT1*, and *PTEN* (*20*). We transfected these cells with siRNA against *TP53*, *PTEN*, or *FAT1* (fig. S6A) or treated them with EGF (1 μg/ml) for 24 hours. All of these cultures increased their expression and/or activation of YAP1 as determined by immunoblotting to measure YAP1/glyceraldehyde-3-phosphate dehydrogenase (GAPDH) and/or YAP1/phosphorylated YAP1 (pYAP1) ratios (Fig. 6, A and B, and fig. S6B). Nuclear YAP1 protein was also enhanced in these manipulated cells as detected by IF staining (Fig. 6C and fig. S6C). We next investigated the expression of *CTGF*, *BIRC5*, and *TOP2A*, which are major downstream targets of YAP1, and found that their mRNA levels were increased either by the silencing of *TP53*, *PTEN*, or *FAT1* or by EGF treatment (fig. S7A). To confirm our results in another cell line derived from HPV (−) OSCC, we subjected Cal27 cells (*TP53*mt, *PTEN*wt, and *FAT1*wt) to PTEN or FAT1 knockdown, or EGF treatment, and again detected up-regulation of

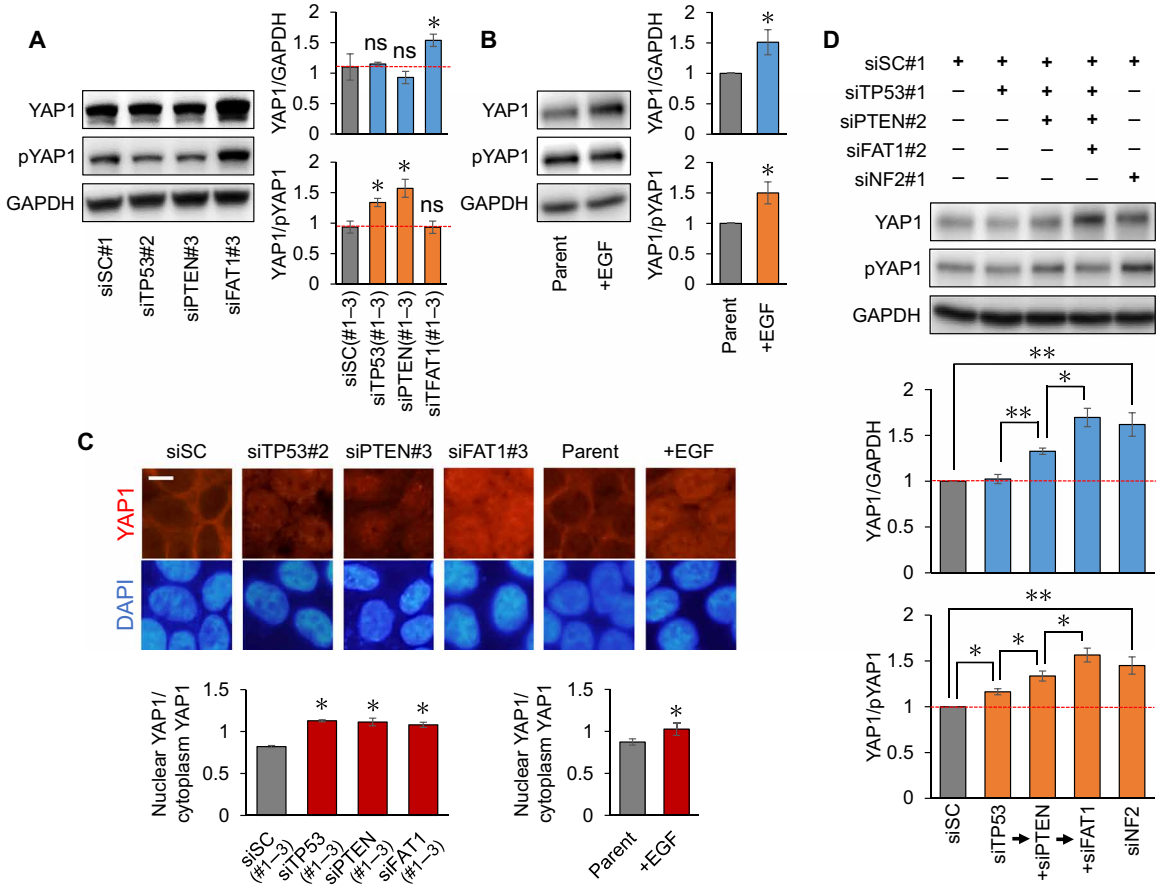

Fig. 6. Molecules that are frequently altered in human HNSCC activate YAP1. (**A** and **B**) Left panels: Immunoblots to detect YAP1 and pYAP1 in WSU-HN30 cells that were either (A) transfected with control siRNA (siSC#1) or with one of three independent siRNAs (#1 to #3) targeting *TP53*, *PTEN*, or *FAT1* or (B) left untreated (Parent) or treated with EGF (1 μg/ml). siRNA- or EGF-treated cells were harvested at 24 or 96 hours after treatment, respectively. Right panels: Ratios of YAP1/GAPDH (protein) and YAP1/pYAP1 (activity) were calculated as described in Materials and Methods. Data are presented as means ± SEM of (A) seven independent siRNA-transfected samples for each gene or (B) three EGF-treated cultures per group. (**C**) Top: IF-based detection (see Supplementary Materials and Methods) of nuclear versus cytoplasmic YAP1 in siRNA-transfected or EGF-treated WSU-HN30 cells treated as in (A) and (B). DAPI (blue), nuclei. Bottom: Ratio of cells with nuclear YAP1/cytoplasmic YAP1 in the top panels. Data are means ± SEM of three independent siRNA-transfected samples for each gene (siRNA transfection) or three cultures treated with EGF. (**D**) Top: Immunoblot to detect YAP1 and pYAP1 in WSU-HN30 cells that were transfected with the indicated siRNAs. Middle and bottom: Ratios of YAP1/GAPDH and YAP1/pYAP1 were analyzed and quantified as in (A) and (B). Data are means ± SEM of four independent experiments involving at least triplicate samples. *$P < 0.05$ and **$P < 0.01$, *t* test.

YAP1 activity (fig. S7, B and C). Moreover, we found a positive correlation between *TP53*mt and YAP1 expression in our human clinical specimens (table S1). Thus, it seems that mutation of any of these tumor suppressor genes and/or increased EGF signaling can upregulate YAP1 expression to some degree in OSCC cells. Intriguingly, some combinations of these gene alterations resulted in YAP1 activation to a high level (Fig. 6D). Thus, an accumulation of these mutations may explain the increased and sustained activation of YAP1 in head-and-neck cancer epithelial cells.

With respect to TP63, *Mob1* deletion enhanced TP63 protein (p63) levels in mouse tongue epithelial cells (fig. S8A), and siRNA-mediated inhibition of *Tp63* expression in SCC9 cells expressing Dox-inducible YAP1-5SA blocked their proliferation (fig. S8B). In addition, overexpression of ΔNp63α only mildly interfered with YAP1 activation in the WSU-HN30 human tongue epithelial cell line (fig. S8, C to E).

The above data collectively indicate that TP53, FAT1, PTEN, and EGFR are all upstream regulators of YAP1, whereas TP63 is a downstream effector of YAP1. These findings prompted us to devise a model in which the mutation (functional inactivation) of *TP53* plus a subset of these genes, including *PIK3CA/PTEN*, *EGFR*, and/or *FAT1*, results in YAP1 hyperactivation that may exceed an oncogenic threshold (fig. S9A). This elevated YAP1 may then activate downstream genes such as Δ*Np63α* and may thereby initiate OSCC onset and/or progression.

DISCUSSION

In this study, we have demonstrated for the first time that YAP1 may be a strikingly potent oncogenic driver of OSCC onset and progression. Cancers usually initiate because of the additive or synergistic effects of several mutated genes that exert their effects during multistep carcinogenesis (*1*). However, because the onset of tongue tumors in our tg*Mob1*DKO mice was so quick, we propose a new concept positing that OSCC may be initiated when sustained YAP1 activity exceeds a particular oncogenic threshold (refer to fig. S9A). Many recent reports have linked YAP1 activation to either loss-of-function (LOF) mutations of key genes such as *TP53* and *FAT1*, or the triggering of pathways related to PI3K/AKT or EGFR (*11*–*14*). We have

confirmed these findings in human OSCC cells (Fig. 6, A to C, and fig. S7) and have established that an accumulation of YAP1 activity can be driven by various combinations of these alterations (Fig. 6D). Depending on the strength of YAP1 activation attributed to one alteration, the oncogenic threshold may be exceeded with only a few additional mutations.

The role of TP53 in OSCC poses an interesting conundrum. LOF of *TP53* inhibits expression of PTPN14 and 14-3-3, which are downstream transcriptional targets of TP53 (*11*, *21*), and so is likely to promote YAP1 activity. However, *TP53* gain-of-function (GOF) mutations (e.g., R248L, R175H, and R273H), which are observed in 9.5% of HNSCCs, reportedly bind directly to and stabilize YAP1 (*22*), also promoting YAP1 activity. The binding of GOF-mutated TP53 to YAP1 can activate transcription factors such as NF-Y, whose target genes act to increase cell proliferation (*23*). Thus, both LOF and GOF mutations of *TP53* can enhance YAP1 activity and so may contribute to human OSCC carcinogenesis. Nevertheless, because mice solely lacking normal TP53 function do not develop OSCC (*6*), there must be other factors required for the onset and development of OSCC.

Repeated exposure to carcinogens (including tobacco and alcohol), irritation of the oral mucosa (especially tongue epithelium) due to the presence of tooth decay, or mechanical stimulation by ill-fitting dentures are the main causes of human OSCC (*1*, *24*). These events may also directly activate YAP1 or induce oncogenic mutations in the abovementioned genes that activate YAP1. Cigarette smoke extract (*25*) and mechanical stimulation (*26*) have both been shown to activate YAP1 in various cell types, including in esophageal and cervical cells. These observations support our hypothesis that OSCC is caused by the boosting of YAP1 activity over a certain threshold. Furthermore, although YAP1 protein itself is frequently activated and accumulates in most tumors (*8*), the actual DNA mutation of Hippo-related genes, including *YAP1*, is relatively rare in cancers (*27*). Thus, our work erases many years of doubt as to how HNSCCs can arise in the absence of GOF mutations of major oncogenes (*28*).

One possible reason for the frequent and early onset of OSCC in our mutant mice is the activation of ΔNp63, a master regulator of epidermal keratinocyte proliferation and differentiation (*29*). Activated YAP1 binds directly to ΔNp63 protein and stabilizes it (*30*). A lack of TP63 in mice results in the absence of the epidermis and its related appendages (*29*), and *Tp63*-deficient embryonic stem cells exhibit up-regulation of mesodermal genes (*31*). Conversely, overexpression of ΔNp63 in the presence of KLF4 induces the conversion of fibroblasts to cells of the keratinocyte lineage (*32*). We found that TP63 accumulated in tongue epithelial cells in our mouse model of OSCC (fig. S8A). Last, we demonstrated that inhibition of ΔNp63 expression blocked the cell proliferation induced by YAP1 overexpression (fig. S8B). We speculate that hyperactivation of YAP1 leading to high levels of stabilized ΔNp63 may both skew cells toward the keratinocyte lineage and boost keratinocyte proliferation and dedifferentiation, which may, in turn, increase the chance of OSCC development. A second reason for the early onset of invasive SCC in our mutant mice may be increased production of BMP4. BMP4 is a soluble growth factor that plays an essential role in epidermal development by regulating ΔNp63 (*33*). High levels of BMP4 were detected in tg*Mob1*DKO tongue epithelial cells compared to controls when examined by microarray analysis (fig. S9B). A third possible reason for our observations may be the existence of positive feedback between EGF signaling and YAP1. YAP1 increases the transcription of EGF receptors (EGFR and ERBB3) and EGF-like ligands (HBEGF, NRG1, and NRG2) (*16*). Conversely, both HBEGF and NRG1 have been shown to activate YAP1 in ovarian cancer (*14*). Although we did not observe a significant increase in *EGFR*, *ERBB3*, or *HBEGF* mRNAs when MOB1 was deleted (YAP1 activated) in mouse tongue epithelium, we did detect elevation of *NRG1/2* mRNAs (fig. S9B), suggesting the existence of an NRG1/2-(ERBB3)-YAP1-NRG1/2 autocrine loop that controls OSCC tumorigenesis and progression. All three of these mechanisms may contribute to OSCC genesis, perhaps explaining why the phenotype is so strong, especially in epidermal cells.

An important finding emerging from our study is that mice lacking MOB1 plus TAZ developed more aggressive invasive SCC than did mice lacking MOB1 alone. This result indicates that YAP1 and TAZ may be activated independently in the SCC context and that the mechanism by which MOB1A/B regulates YAP1 differs from its effects on TAZ in these malignancies. Further study will be required to understand and distinguish between the underlying molecular mechanisms. Nevertheless, our data imply that selective targeting of YAP1 may be an effective new mode of OSCC treatment.

Two TAM-inducible epidermal SCC models have been previously described. In the first model, the mutant mice bear a *K-Ras* transgene and an inducible *Tp53* KO gene (*34*). Half of these mutants develop skin SCCs by 35 weeks after TAM. In the second model, the mice bear an *AKT* transgene and an inducible *Tp53* KO gene, leading to HNSCC development in 50% of animals by 35 weeks after TAM (*35*). Thus, we were greatly surprised to observe CIS in the tongue as early as 1 week after TAM in our tg*Mob1*DKO mutants, followed by the inevitable development of invasive SCC by 4 weeks after TAM. Considering that it takes more than 7 days to completely inhibit MOB1 protein expression (fig. S1C), it seems that *Mob1a/b*-deficient keratinocytes (which bear disruption of a single pathway) may become cancerous immediately without undergoing any other molecular alterations. Our mutant mice thus currently constitute the world's fastest spontaneous cancer onset model. Moreover, cancer progression is synchronized in all these mutants, and the tumors are easily visualized on the mouse exterior. These characteristics make our model a particularly attractive tool for cancer research and the development of new anticancer drugs. This latter point is a pressing issue because, in the past, several dose-intensified chemo/radiotherapy trials were conducted for HNSCC treatment but quickly reached the limit of human tolerance, showing positive results for only a few select patients (*3*). Furthermore, recurrent and metastatic HNSCCs are refractory to both conventional chemotherapies and currently available molecular targeting drugs such as EGFR inhibitor (cetuximab) or anti-PD1 antibody (nivolumab), which only marginally improve patient survival (*4*). Our work has shown that inhibition of YAP1 not only prevents the onset of OSCC but also slows its progression. YAP1 may thus be an appealing molecular target for therapy of this devastating disease. We expect to use our mutant mice to identify new drugs targeting the Hippo pathway in epidermal cancers, including in HNSCCs, with the goal of bringing concrete benefits to patients.

MATERIALS AND METHODS

Parental mouse strains and cell lines

Previously established mouse strains used in this study were *Mob1a*$^{flox/flox}$; *Mob1b*$^{-/-}$ (*17*), *Rosa26-CreERT* (The Jackson Laboratory), and *Taz*$^{flox/flox}$ (provided by J. Wrana). *Yap1*$^{flox/flox}$ mice were generated using *Yap1*$^{flox/flox}$ embryonic stem cells from the Knockout Mouse Project Repository

(*36*). All mice were kept in specific pathogen–free facilities at Kobe and Kyushu Universities.

Human tongue SCC cell lines HSC3, HSC4, and SCC4 (all from the Japanese Collection of Research Bioresources); SCC9 and Cal27 (both from the American Type Culture Collection); WSU-HN30 (provided by S. Gutkind, University of California); and H1299-Luc (established by H.H.) were cultured in Eagle's minimum essential medium, Dulbecco's modified Eagle's medium (DMEM), DMEM/Ham's F12 medium, or RPMI medium, respectively, supplemented with 10% heat-inactivated fetal bovine serum and 1% penicillin-streptomycin at 37°C in a 5% CO_2/95% air incubator. Hydrocortisone (400 ng/ml) was added to the medium of SCC4 and SCC9 cultures, in line with a standard protocol.

Generation of *Mob1a/b* DKO mice and related strains

Mob1a/b homozygous double-mutant mice (*Rosa26-CreERT*; $Mob1a^{flox/flox}$; $Mob1b^{-/-}$) were generated by mating *Rosa26-CreERT* Tg mice with $Mob1a^{flox/flox}$; $Mob1b^{-/-}$ mice. *Rosa26-CreERT* Tg mice were in a C57BL/6 background, and $Mob1a^{flox/flox}$; $Mob1b^{-/-}$ mice were backcrossed to C57BL/6 for more than six generations. To delete the floxed *Mob1a* gene, TAM (Sigma-Aldrich) diluted in 100% ethanol (10 mg/ml) was applied daily directly to the mouse tongue for 5 days by brush. The area of application is indicated in fig. S1A. Before TAM application, mice were anesthetized with a mixture of medetomidine hydrochloride, midazolam, and butorphanol. $Mob1a^{flox/flox}$; $Mob1b^{-/-}$ mice treated with TAM were used as controls unless otherwise stated. *Rosa26-CreERT*; $Mob1a^{flox/flox}$; $Mob1b^{-/-}$; $Yap1^{flox/flox}$ and *Rosa26-CreERT*; $Mob1a^{flox/flox}$; $Mob1b^{-/-}$; $Taz^{flox/flox}$ mice were generated by mating *Rosa26-CreERT*; $Mob1a^{flox/flox}$; $Mob1b^{-/-}$ mice with $Yap1^{flox/flox}$ or $Taz^{flox/flox}$ mice, respectively.

The primers used for mouse genotyping polymerase chain reaction were as follows: $Mob1a^{wt/flox}$, GTCTCGTGAAGGGTCTTGAGG/CCTGGTTGGGGTGGAGAATCAA [wt, 319 base pairs (bp); flox, 450 bp]; $Mob1a^{\Delta}$, GTAATGTGTTCAGCTATGCTTTGAC/CCTGGTTGGGGTGGAGAATCAA (551 bp); $Mob1b^{wt}$, CTTCAGGATCCTTGGTGGTTATCAG/AGAGCAAGGGGAAAAGAAGCTCAATG (586 bp); $Mob1b^{mutant}$, CTTCAGGATCCTTGGTGGTTATCAG/TCAGGGTCACAAGGTTCATATGGTG (673 bp); *Rosa26-CreERT Tg*, AAAGTCGCTCTGAGTTGTTAT/CCTGATCCTGGCAATTTCG (825 bp); $Yap1^{wt/flox}$, GCCCAAACATACCCACGTAAT/CAGTCCAGTCAAGACAAGAT (wt, 192 bp; flox, 336 bp); $Taz^{wt/flox}$, AAGCAGTTTCCACTTCATGAAAC/AGTCAAGAGGGGCAAAGTTGTGA (wt, 250 bp; flox, 330 bp).

Tumor analyses

Tumor tissues were fixed in 4% paraformaldehyde (PFA) in phosphate-buffered saline (PBS) and embedded in paraffin. Sections (4 μm) of tumors were cut for hematoxylin and eosin (H&E) staining. Diagnoses of tongue epithelial dysplasia, CIS, or invasive SCC were confirmed by two pathologists.

Isolation of mouse tongue epithelial cells

Primary tongue epithelium from 3-week-old *Rosa26-CreERT*; $Mob1a^{flox/flox}$; $Mob1b^{-/-}$ mice without TAM was obtained using a dermal keratinocyte isolation protocol (*37*). Briefly, resected tongue tissues were placed into ice-cold dispase digestion buffer [250 U of dispase (Godo Shusei) in PBS] and incubated overnight at 4°C. The epidermis was slowly separated from the dermis using forceps and floated on trypsin solution (Gibco) at room temperature for 40 min to create a primary tongue epithelial cell suspension. Tongue epithelial cells were cultured in CnT-PR medium (CELLnTEC) and passaged more than 40 times to generate the *iMob1*DKO tongue epithelial cell line. Loss of *Mob1a/b* in these cells in vitro was induced by treating them with TAM (0.5 μM; Toronto Research Chemicals) for 3 days.

Immunoblotting

Immunoblotting was carried out using a standard protocol and primary antibodies recognizing MOB1A (#E1N9D; Cell Signaling Technology), MST1 (#3682S; Cell Signaling Technology), LATS1 (C66B5; Cell Signaling Technology), YAP1 (#4912S; Cell Signaling Technology), pYAP1(S127) (#4911S; Cell Signaling Technology), TAZ (V386; Cell Signaling Technology), pTAZ (S89) (#75275; Cell Signaling Technology), CTGF (L-20; Santa Cruz Biotechnology), BIRC5 (71G4B7; Cell Signaling Technology), TOP2A (EP1102Y; Abcam), or TP63 (4A4; Abcam). Primary antibodies were detected using horseradish peroxidase (HRP)–conjugated secondary rabbit antibody (#7074; Cell Signaling Technology). Endogenous GAPDH (FL-355; Santa Cruz Biotechnology) was used as the internal control. Quantification of signal intensity was performed using Fujifilm Multi Gauge software.

Immunostaining

Mice tongue tissues were fixed in 4% PFA, embedded in paraffin, and sectioned (4 μm) using standard procedures. IHC or IF staining was performed using an indirect method using primary antibodies recognizing YAP1 (WH0010413M1; Sigma), Ki67 (ab15580; Abcam), or TP63 (4A4; Abcam). Primary antibodies were detected using REAL EnVision HRP-rabbit/mouse (Dako) or Alexa Fluor 568 (Molecular Probes). Some slides were counterstained with Mayer's hematoxylin (Muto) or 4′,6-diamidino-2-phenylindole (DAPI; Dojindo) before mounting using PermaFluor (Thermo Scientific). For Ki67 positivity studies, 200 cells per mouse were examined.

Clinical samples

From the population of patients who were treated at the National Hospital Organization Kyushu Cancer Center in Japan from 2008 to 2013, we selected 86 patients who had received surgical resection of tongue SCC as their first line of therapy and performed a retrospective review of their medical charts. Their resected cancer tissues (n = 86), which had been fixed in formalin, were stained with antibodies recognizing: YAP1 (WH0010413M1; Sigma), TP53 (DO7; Sigma), CTGF (ab6992; Abcam), BIRC5 (EP2880Y; Abcam), or TOP2A (TOP2A/1362; Abcam). Within these stained resected tissues, areas of NT epithelium, dysplasia, CIS, or invasive SCC were determined and levels of YAP1 activity (grade) were scored. YAP1 grade was defined by multiplying the "YAP1 frequency score" by the "YAP1 intensity score," as previously described (*38*). A score of >8 classified a sample into the YAP1-high group.

To compare overall survival and relapse-free survival rates between groups of patients with high (n = 14) or low (n = 72) YAP1 expression, Kaplan-Meier curves were generated and a Wilcoxon test was used to analyze statistical differences. Overall survival was calculated on the basis of the length of time between date of surgery and date of death. Follow-up duration was 68.1 months on average (range of 3 to 128 months).

To investigate factors influencing YAP1 activity, the following clinicopathological factors were included in the univariate analyses: age, sex, history of smoking, history of alcohol, T stage (which describes the primary tumor size and site), N stage (which describes

the degree of regional lymph node involvement), clinical stage, recurrence, degree of tumor differentiation, presence of multiple cancers, and *TP53* mutation status [defined as previously described (*39*)] (see table S1). Univariate analyses were performed using the chi-square test.

siRNA transfection

siRNA targeting of *YAP1*, *TP53*, *PTEN*, *FAT1*, or *NF2* expression was performed using siRNA oligonucleotides of the following sequences: si-scramble #1, CGUACGCGGAAUACUUCGA; si-scramble #2, UUCUCCGAACGUGUGUCACGU; si-scramble #3, siNC1 (Ambion); si-*YAP1* #1, GGCCCUUUGAUUUAGUAUA; si-*TP53* #1, GUAAUCUACUGGGACGGAA; si-*TP53* #2, GAAAUUUGCGUGUGGAGUA; si-*TP53* #3, GGUGAACCUUAGUACCUAA; si-*PTEN* #1, GCAUACGAUUUUAAGCGGA; si-PTEN #2, CACCGCAUAUUAAAACGUA; si-*PTEN* #3, CAAGAAAUCGAUAGCAUUU; si-*FAT1* #1, GGACCGAAAUUCCUUCGAA; si-*FAT1* #2, CGGAAGUUAUCGUUCCGAU; si-*FAT1* #3, GACCGAAAUUCCUUCGAA; si-*NF2* #1, CAAGCACAAUACCAUUAAA; si-*NF2* #2, CCCAAGACGACGUUCACCGUGA; si-*NF2* #3, AGAAGCAGAUUUUAGAUGA; si-*TP63*#1, GAACCGCCGUCCAAUUUUA; and si-*TP63*#2, UGAUGAACUGUUAUACUUA.

Transfection of siRNA oligonucleotides (10 nM) into exponentially growing WSU-HN30 tongue cancer cells was performed using Lipofectamine RNAiMAX (Invitrogen) following the manufacturer's protocol. At 96 hours after transfection, protein lysates were subjected to immunoblotting and cells were IF-stained to detect YAP1 as described above.

EGF treatment

WSU-HN30 cells (2×10^5) were seeded in six-well plates. After 48 hours, EGF (1 μg/ml; PeproTech) was added to the culture medium and cells were incubated for 24 hours before harvesting. Immunoblotting and IF staining to detect YAP1 were conducted as described above.

In vitro effects of YAP1-targeting drugs

To determine the in vitro effects of drugs known to target YAP1, HSC4 cells (1×10^4 per well in 24-well plates) were cultured for 1 to 3 days in DMEM/Ham's F12 medium containing 5 μM dasatinib (Abcam), 5 μM verteporfin (USP), 5 μM simvastatin (TCI), or vehicle (DMSO; negative control). Inhibition of cell growth was assessed by counting cell numbers per well.

In vivo effects of dasatinib and simvastatin

To determine the in vivo effects of dasatinib and simvastatin on the initiation and progression of tongue cancer in tg*Mob1*DKO mice, dasatinib (5 mg/kg, intraperitoneally), simvastatin (50 mg/kg, intraperitoneally), or vehicle (DMSO; negative control) was administered daily for 14 to 17 days starting either 3 days before TAM application (for Fig. 4A) or after CIS onset starting at 2 weeks after TAM (for Fig. 4J).

Tumor growth in xenografted *nude* mice

To determine the effect of YAP1 silencing in vivo, human tongue SCC cells (HSC4; 1×10^7) that had been transfected with Dox-dependent shYAP1 were injected subcutaneously into the flanks of 9-week-old female BALB/cAJcl-*nu/nu* mice (CLEA Japan). After visual detection of tumors (usually at 10 days after injection), mice were supplied with normal drinking water or water containing Dox (2 mg/ml). To determine the in vivo effects of dasatinib on human tongue SCC cells, nontransfected HSC4 cells (1×10^7) were injected subcutaneously into *nude* mice as above. After visual detection of tumors (usually at 10 days after injection), mice were treated daily with dasatinib (5 mg/kg, intraperitoneally) or vehicle (DMSO; negative control). In both cases, tumor volumes were measured every 4 days using calipers.

Statistics

Unless otherwise indicated, all results represent the mean ± SEM. Statistical comparisons between different groups were performed using the two-tailed Student's *t* test. For all statistical analyses, differences of $P < 0.05$ were considered statistically significant. All experiments were repeated at least three times.

Study approval

Animal experiments were approved by the Kobe University (#P170604) and Kyushu University (#28-156) Animal Experiment Committees, and the care of the animals was in accordance with institutional guidelines. All clinical samples were approved for analysis by the Ethics Committee at the National Hospital Organization Kyushu Cancer Center (#2015-43). Written informed consent was obtained from all patients whose cancers were analyzed in this study.

SUPPLEMENTARY MATERIALS

Supplementary material for this article is available at http://advances.sciencemag.org/cgi/content/full/6/12/eaay3324/DC1

Supplementary Materials and Methods

Table S1. Clinicopathological features of 86 cases of human tongue squamous cell carcinoma.

Fig. S1. Induction of *Mob1a/b* deletion in tg*Mob1*DKO mice by postnatal application of TAM.

Fig. S2. Cell-cell junction collapse and retained cell size of *iMob1*DKO cells and YAP1/TAZ expression and localization in tongue epithelium of tg*Mob1*DKO, tg*Yap1*TKO, and tg*Taz*TKO mice.

Fig. S3. Effects of dasatinib, simvastatin, verteporfin, and Y-27632 on YAP1 protein expression and activation and tumor-suppressive effect of simvastatin.

Fig. S4. YAP1 expression in OSCC cell lines, the effect on an OSCC cell line of YAP1 depletion combined with cisplatin, and the effect of dasatinib on cell death in tg*Mob1*DKO mice.

Fig. S5. YAP1 target gene expression correlates with YAP1 nuclear expression in human clinical OSCC specimens.

Fig. S6. Evaluation of gene knockdown and ectopic gene expression in the WSU-HN30 HNSCC cell line and activation of YAP1 by knockdown of *TP53*, *PTEN*, or *FAT1*.

Fig. S7. Activation of YAP1 target gene expression by molecules that are frequently altered in human OSCC.

Fig. S8. Positive correlation of ΔNp63α protein expression with YAP1 protein expression.

Fig. S9. Graphical abstract and microarray analysis of growth factors and receptors whose mRNAs are up-regulated in tg*Mob1*DKO tongue epithelial cells.

References (*40*, *41*)

View/request a protocol for this paper from *Bio-protocol*.

REFERENCES AND NOTES

1. C. R. Leemans, P. J. F. Snijders, R. H. Brakenhoff, Publisher correction: The molecular landscape of head and neck cancer. *Nat. Rev. Cancer* **18**, 662 (2018).
2. Cancer Genome Atlas Network, Comprehensive genomic characterization of head and neck squamous cell carcinomas. *Nature* **517**, 576–582 (2015).
3. J. Corry, L. J. Peters, D. Rischin, Optimising the therapeutic ratio in head and neck cancer. *Lancet Oncol.* **11**, 287–291 (2010).
4. A. Argiris, K. J. Harrington, M. Tahara, J. Schulten, P. Chomette, A. Ferreira Castro, L. Licitra, Evidence-based treatment options in recurrent and/or metastatic squamous cell carcinoma of the head and neck. *Front. Oncol.* **7**, 72 (2017).
5. M. Thomas, D. Pim, L. Banks, The role of the E6-p53 interaction in the molecular pathogenesis of HPV. *Oncogene* **18**, 7690–7700 (1999).
6. W. Supsavhad, W. P. Dirksen, C. K. Martin, T. J. Rosol, Animal models of head and neck squamous cell carcinoma. *Vet. J.* **210**, 7–16 (2016).
7. M. Nishio, T. Maehama, H. Goto, K. Nakatani, W. Kato, H. Omori, Y. Miyachi, H. Togashi, Y. Shimono, A. Suzuki, Hippo vs. Crab: Tissue-specific functions of the mammalian Hippo pathway. *Genes Cells* **22**, 6–31 (2017).
8. F. Zanconato, M. Cordenonsi, S. Piccolo, YAP/TAZ at the roots of cancer. *Cancer Cell* **29**, 783–803 (2016).

9. Y.-G. Eun, D. Lee, Y. C. Lee, B. H. Sohn, E. H. Kim, S. Y. Yim, K. H. Kwon, J.-S. Lee, Clinical significance of YAP1 activation in head and neck squamous cell carcinoma. *Oncotarget* **8**, 111130–111143 (2017).
10. S. E. Hiemer, L. Zhang, V. K. Kartha, T. S. Packer, M. Almershed, V. Noonan, M. Kukuruzinska, M. V. Bais, S. Monti, X. Varelas, A YAP/TAZ-regulated molecular signature is associated with oral squamous cell carcinoma. *Mol. Cancer Res.* **13**, 957–968 (2015).
11. S. S. Mello, L. J. Valente, N. Raj, J. A. Seoane, B. M. Flowers, J. McClendon, K. T. Bieging-Rolett, J. Lee, D. Ivanochko, M. M. Kozak, D. T. Chang, T. A. Longacre, A. C. Koong, C. H. Arrowsmith, S. K. Kim, H. Vogel, L. D. Wood, R. H. Hruban, C. Curtis, L. D. Attardi, A p53 super-tumor suppressor reveals a tumor suppressive p53-Ptpn14-Yap axis in pancreatic cancer. *Cancer Cell* **32**, 460–473.e6 (2017).
12. R. García-Escudero, C. Segrelles, M. Dueñas, M. Pombo, C. Ballestín, M. Alonso-Riaño, P. Nenclares, R. Álvarez-Rodríguez, G. Sánchez-Aniceto, A. Ruíz-Alonso, J. L. López-Cedrún, J. M. Paramio, C. Lorz, Overexpression of PIK3CA in head and neck squamous cell carcinoma is associated with poor outcome and activation of the YAP pathway. *Oral Oncol.* **79**, 55–63 (2018).
13. D. Martin, M. S. Degese, L. Vitale-Cross, R. Iglesias-Bartolome, J. L. C. Valera, Z. Wang, X. Feng, H. Yeerna, V. Vadmal, T. Moroishi, R. F. Thorne, M. Zaida, B. Siegele, S. C. Cheong, A. A. Molinolo, Y. Samuels, P. Tamayo, K. L. Guan, S. M. Lippman, J. G. Lyons, J. S. Gutkind, Assembly and activation of the Hippo signalome by FAT1 tumor suppressor. *Nat. Commun.* **9**, 2372 (2018).
14. C. He, X. Lv, G. Hua, S. M. Lele, S. Remmenga, J. Dong, J. S. Davis, C. Wang, YAP forms autocrine loops with the ERBB pathway to regulate ovarian cancer initiation and progression. *Oncogene* **34**, 6040–6054 (2015).
15. R. Ehsanian, M. Brown, H. Lu, X. P. Yang, A. Pattatheyil, B. Yan, P. Duggal, R. Chuang, J. Doondeea, S. Feller, M. Sudol, Z. Chen, C. Van Waes, YAP dysregulation by phosphorylation or ΔNp63-mediated gene repression promotes proliferation, survival and migration in head and neck cancer subsets. *Oncogene* **29**, 6160–6171 (2010).
16. S. V. Saladi, K. Ross, M. Karaayvaz, P. R. Tata, H. Mou, J. Rajagopal, S. Ramaswamy, L. W. Ellisen, ACTL6A is co-amplified with p63 in squamous cell carcinoma to drive YAP activation, regenerative proliferation, and poor prognosis. *Cancer Cell* **31**, 35–49 (2017).
17. M. Nishio, K. Hamada, K. Kawahara, M. Sasaki, F. Noguchi, S. Chiba, K. Mizuno, S. O. Suzuki, Y. Dong, M. Tokuda, T. Morikawa, H. Hikasa, J. Eggenschwiler, N. Yabuta, H. Nojima, K. Nakagawa, Y. Hata, H. Nishina, K. Mimori, M. Mori, T. Sasaki, T. W. Mak, T. Nakano, S. Itami, A. Suzuki, Cancer susceptibility and embryonic lethality in Mob1a/1b double-mutant mice. *J. Clin. Invest.* **122**, 4505–4518 (2012).
18. J. C. Montero, S. Seoane, A. Ocaña, A. Pandiella, Inhibition of SRC family kinases and receptor tyrosine kinases by dasatinib: Possible combinations in solid tumors. *Clin. Cancer Res.* **17**, 5546–5552 (2011).
19. K. Nakatani, T. Maehama, M. Nishio, H. Goto, W. Kato, H. Omori, Y. Miyachi, H. Togashi, Y. Shimono, A. Suzuki, Targeting the Hippo signalling pathway for cancer treatment. *J. Biochem.* **161**, 237–244 (2017).
20. D. Martin, M. C. Abba, A. A. Molinolo, L. Vitale-Cross, Z. Wang, M. Zaida, N. C. Delic, Y. Samuels, J. G. Lyons, J. S. Gutkind, The head and neck cancer cell oncogenome: A platform for the development of precision molecular therapies. *Oncotarget* **5**, 8906–8923 (2014).
21. N. Furth, Y. Aylon, M. Oren, p53 shades of Hippo. *Cell Death Differ.* **25**, 81–92 (2018).
22. L. Verduci, M. Ferraiuolo, A. Sacconi, F. Ganci, J. Vitale, T. Colombo, P. Paci, S. Strano, G. Macino, N. Rajewsky, G. Blandino, The oncogenic role of circPVT1 in head and neck squamous cell carcinoma is mediated through the mutant p53/YAP/TEAD transcription-competent complex. *Genome Biol.* **18**, 237 (2017).
23. S. Di Agostino, G. Sorrentino, E. Ingallina, F. Valenti, M. Ferraiuolo, S. Bicciato, S. Piazza, S. Strano, G. Del Sal, G. Blandino, YAP enhances the pro-proliferative transcriptional activity of mutant p53 proteins. *EMBO Rep.* **17**, 188–201 (2016).
24. E. Piemonte, J. Lazos, P. Belardinelli, D. Secchi, M. Brunotto, H. Lanfranchi-Tizeira, Oral cancer associated with chronic mechanical irritation of the oral mucosa. *Med. Oral Patol. Oral Cir. Bucal* **23**, e151–e160 (2018).
25. L. John, G. Sharma, S. P. Chaudhuri, B. Pillai, Cigarette smoke extract induces changes in growth and gene expression of Saccharomyces cerevisiae. *Biochem. Biophys. Res. Commun.* **338**, 1578–1586 (2005).
26. A. Elbediwy, Z. I. Vincent-Mistiaen, B. J. Thompson, YAP and TAZ in epithelial stem cells: A sensor for cell polarity, mechanical forces and tissue damage. *Bioessays* **38**, 644–653 (2016).
27. F. X. Yu, B. Zhao, K. L. Guan, Hippo pathway in organ size control, tissue homeostasis, and cancer. *Cell* **163**, 811–828 (2015).
28. M. Masuda, T. Wakasaki, S. Toh, Stress-triggered atavistic reprogramming (STAR) addiction: Driving force behind head and neck cancer? *Am. J. Can. Res.* **6**, 1149–1166 (2016).
29. G. Melino, E. M. Memmi, P. G. Pelicci, F. Bernassola, Maintaining epithelial stemness with p63. *Sci. Signal.* **8**, re9 (2015).
30. A. Chatterjee, T. Sen, X. Chang, D. Sidransky, Yes-associated protein 1 regulates the stability of ΔNp63α. *Cell Cycle* **9**, 162–167 (2010).
31. A. Medawar, T. Virolle, P. Rostagno, S. de la Forest-Divonne, K. Gambaro, M. Rouleau, D. Aberdam, ΔNp63 is essential for epidermal commitment of embryonic stem cells. *PLOS ONE* **3**, e3441 (2008).
32. Y. Chen, D. S. Mistry, G. L. Sen, Highly rapid and efficient conversion of human fibroblasts to keratinocyte-like cells. *J. Invest. Dermatol.* **134**, 335–344 (2014).
33. C. Tribulo, M. Guadalupe Barrionuevo, T. H. Agüero, S. S. Sánchez, N. B. Calcaterra, M. J. Aybar, ΔNp63 is regulated by BMP4 signaling and is required for early epidermal development in Xenopus. *Dev. Dyn.* **241**, 257–269 (2012).
34. C. Caulin, T. Nguyen, G. A. Lang, T. M. Goepfert, B. R. Brinkley, W.-W. Cai, G. Lozano, D. R. Roop, An inducible mouse model for skin cancer reveals distinct roles for gain- and loss-of-function p53 mutations. *J. Clin. Invest.* **117**, 1893–1901 (2007).
35. M. Moral, C. Segrelles, M. F. Lara, A. B. Martínez-Cruz, C. Lorz, M. Santos, R. García-Escudero, J. Lu, K. Kiguchi, A. Buitrago, C. Costa, C. Saiz, J. L. Rodriguez-Peralto, F. J. Martinez-Tello, M. Rodriguez-Pinilla, M. Sanchez-Cespedes, M. Garín, T. Grande, A. Bravo, J. DiGiovanni, J. M. Paramio, Akt activation synergizes with Trp53 loss in oral epithelium to produce a novel mouse model for head and neck squamous cell carcinoma. *Cancer Res.* **69**, 1099–1108 (2009).
36. H. Goto, M. Nishio, Y. To, T. Oishi, Y. Miyachi, T. Maehama, H. Nishina, H. Akiyama, T. W. Mak, Y. Makii, T. Saito, A. Yasoda, N. Tsumaki, A. Suzuki, Loss of Mob1a/b in mice results in chondrodysplasia due to YAP1/TAZ-TEAD-dependent repression of SOX9. *Development* **145**, dev159244 (2018).
37. U. Lichti, J. Anders, S. H. Yuspa, Isolation and short-term culture of primary keratinocytes, hair follicle populations and dermal cells from newborn mice and keratinocytes from adult mice for in vitro analysis and for grafting to immunodeficient mice. *Nat. Protoc.* **3**, 799–810 (2008).
38. M. Nishio, K. Sugimachi, H. Goto, J. Wang, T. Morikawa, Y. Miyachi, Y. Takano, H. Hikasa, T. Itoh, S. O. Suzuki, H. Kurihara, S. Aishima, A. Leask, T. Sasaki, T. Nakano, H. Nishina, Y. Nishikawa, Y. Sekido, K. Nakao, K. Shin-ya, K. Mimori, A. Suzuki, Dysregulated YAP1/TAZ and TGF-β signaling mediate hepatocarcinogenesis in Mob1a/1b-deficient mice. *Proc. Natl. Acad. Sci. U.S.A.* **113**, E71–E80 (2016).
39. A. Yemelyanova, R. Vang, M. Kshirsagar, D. Lu, M. A. Marks, I. M. Shih, R. J. Kurman, Immunohistochemical staining patterns of p53 can serve as a surrogate marker for TP53 mutations in ovarian carcinoma: An immunohistochemical and nucleotide sequencing analysis. *Mod. Pathol.* **24**, 1248–1253 (2011).
40. C. Riccardi, I. Nicoletti, Analysis of apoptosis by propidium iodide staining and flow cytometry. *Nat. Protoc.* **1**, 1458–1461 (2006).
41. M. Sasaki, K. Kawahara, M. Nishio, K. Mimori, R. Kogo, K. Hamada, B. Itoh, J. Wang, Y. Komatsu, Y. R. Yang, H. Hikasa, Y. Horie, T. Yamashita, T. Kamijo, Y. Zhang, Y. Zhu, C. Prives, T. Nakano, T. W. Mak, T. Sasaki, T. Maehama, M. Mori, A. Suzuki, Regulation of the MDM2-P53 pathway and tumor growth by PICT1 via nucleolar RPL11. *Nat. Med.* **17**, 944–951 (2011).

Acknowledgments: We thank H. Togashi, Y. Shimono, and K. Okada (all of Kobe University) for expert technical assistance and critical discussions. We thank J. Wrana (Lunenfeld-Tanenbaum Research Institute) for *Taz*$^{flox/flox}$ mice and J. S. Gutkind (University of California) for WSU-HN30 cells. **Funding:** We are grateful for the funding provided by the Japanese Society for the Promotion of Science (JSPS; grants 17H01400, 26114005, and 26640081 to A.S.); the Cooperative Research Project Program of the Medical Institute of Bioregulation, Kyushu University; Nanken-Kyoten, Tokyo Medical and Dental University (TMDU); the Project for Development of Innovative Research on Cancer Therapeutics (P-DIRECT; grant 11088019 to A.S.); the Japanese Agency for Medical Research and Development [P-CREATE (AMED); grant JP19cm0106114 to A.S.]; the Uehara Memorial Foundation (to A.S.); the Shinnihon Advanced Medical Research Foundation (to A.S.); the Daiichi-Sankyo Scholarship Donation Program (to A.S.). **Author contributions:** Conceptualization: H.O., M.N., T.M., and A.S.; analysis: H.O., M.N., T.M., Y.M., F.U., T. Nakano, and K.T.; resources: H.H., H.N., T.K., and M.M.; data curation: T. Nakano, K.S., K.M., and H.T.; writing of the original draft: H.O., T.M., and A.S.; supervision: M.M., K.M., T.W.M., K.N., and T. Nakagawa; project administration: T.M. and A.S.; funding acquisition: A.S. **Competing interests:** The authors declare that they do not have competing interest. **Data and materials availability:** All data needed to evaluate the conclusions in the paper are present in the paper and/or the Supplementary Materials. Additional data related to this paper may be requested from the authors.

Submitted 12 June 2019
Accepted 18 December 2019
Published 18 March 2020
10.1126/sciadv.aay3324

Citation: H. Omori, M. Nishio, M. Masuda, Y. Miyachi, F. Ueda, T. Nakano, K. Sato, K. Mimori, K. Taguchi, H. Hikasa, H. Nishina, H. Tashiro, T. Kiyono, T. W. Mak, K. Nakao, T. Nakagawa, T. Maehama, A. Suzuki, YAP1 is a potent driver of the onset and progression of oral squamous cell carcinoma. *Sci. Adv.* **6**, eaay3324 (2020).